Structure and Optical Spectroscopy of [Rh(2-phenylpyridine)$_2$(2,2'-bipyridine)]PF_6 and Related Complexes

Gabriela Frei,[†] Arne Zilian,[†] Andrea Raselli,[‡] Hans U. Güdel,*[,†] and Hans-Beat Bürgi[‡]

Institut für Anorganische, Analytische und Physikalische Chemie, Universität Bern, Freiestrasse 3, 3000 Bern 9, Switzerland, and Laboratorium für Kristallographie, Universität Bern, Freiestrasse 3, 3000 Bern 9, Switzerland

Received January 31, 1992

The crystal structure of [Rh(phpy)$_2$(bpy)]PF_6 (phpyH = 2-phenylpyridine, bpy = 2,2'-bipyridine) is determined and described. Crystallographic data at 100 K: chemical formula $C_{32}H_{24}F_6N_4PRh$, orthorhombic crystal system, space group *Pbca* (No. 61), $Z = 8$, $a = 10.821$ (1) Å, $b = 15.798$ (1) Å, $c = 33.328$ (3) Å, $V = 5697.4$ (9) Å^3. There is one complex cation, i.e. two crystallographically inequivalent phpy$^-$ ligands, per asymmetric unit. Polarized single-crystal absorption spectra of [Rh(phpy)$_2$(bpy)]PF_6 and excitation and site-selective luminescence spectra of [Rh(thpy)$_2$(bpy)]$^+$ and [Rh(thpy)(phpy)(bpy)]$^+$ (thpyH = 2-thienylpyridine) doped into [Rh(phpy)$_2$(bpy)]PF_6 are reported and interpreted on the basis of the crystal structure of [Rh(phpy)$_2$(bpy)]PF_6. The two lowest-energy excitations of [Rh(phpy)$_2$(bpy)]PF_6, and also of [Rh(phpy)$_2$(bpy)]BPh_4, [Rh(phpy)$_2$(en)]PF_6, and [Rh(phpy)$_2$(en)]BPh_4 (BPh_4^- = tetraphenylborate anion, en = ethylenediamine), are found in the region between 21 400 and 22 200 cm^{-1} with an energy splitting ranging from 22 to 242 cm^{-1}. They are assigned to electronic transitions involving the phpy$^-$ ligands. The third excited state of [Rh(phpy)$_2$(bpy)]PF_6 lies 967 cm^{-1} above the first excited state and is ascribed to an analogous transition involving the bpy ligand. The polarization properties of these three lowest-energy transitions and the crystal structure of [Rh(phpy)$_2$(bpy)]PF_6 show that the transition moments are parallel to the ligand planes: The bpy transition is short-axis polarized, and the two phpy$^-$ transitions are oriented approximately parallel to the respective Rh–N(phpy$^-$) bonds. It is concluded that the three lowest-energy excited states are essentially $^3\pi\pi^*$ states, localized on the three ligands of the complex. They have a small admixture of the lowest-energy $^1d\pi^*$ excitations through spin–orbit coupling.

1. Introduction

Chelate complexes of d^6 transition metal ions Ru^{2+}, Os^{2+}, Rh^{3+}, and Ir^{3+} with 2,2'-bipyridine (bpy), *o*-phenanthroline, ethylenediamine (en), 2-phenylpyridine anion (phpy$^-$), 2-thienylpyridine anion (thpy$^-$), and similar ligands have found widespread interest, mainly because of their photophysical and photochemical properties and their potential as photocatalysts and photosensitizers.[1] The availability of highly resolved optical spectra from crystalline materials is often helpful for a better understanding of these properties. Only a few of the above complexes have so far been investigated by high-resolution optical spectroscopy. [Ru(bpy)$_3$]$^{2+}$ is one of them, and it is the complex which in the past 15 years has become one of the best known and most widely studied coordination compounds.[2-4] Highly resolved single-crystal absorption spectra at 11 K have also been published for [Rh(phpy)$_2$(bpy)]PF_6 in two different polarizations.[5] They show two dominant electronic origin lines separated by 22 cm^{-1} and associated vibrational sidebands. For a given polarization of the incident light the intensities of these two origin lines and their progressions are comparable. Between the two polarizations there is an intensity ratio of about 1:5 for the spectrum between 22 000 and 26 000 cm^{-1}. In an attempt to interpret these observations, two questions arose: (a) Are the two different origins due to two different sites in the crystal? (b) Can the observed polarization effects be related to the structure and orientation of the complexes in the crystal lattice? We therefore decided to determine the crystal structure of [Rh(phpy)$_2$(bpy)]PF_6, which should answer these questions and provide a basis for a detailed interpretation of further spectroscopic experiments.

Luminescence line narrowing spectroscopy of [Rh(phpy)$_2$(bpy)]$^+$, [Rh(thpy)$_2$(bpy)]$^+$, [Rh(phpy)$_2$(en)]$^+$, and [Rh(thpy)$_2$(en)]$^+$ in glassy matrices has shown that the lowest-energy excited state of these complexes involves one or both of the cyclometalating phpy$^-$ or thpy$^-$ ligands but not the bidentate nitrogen ligand.[6-8] This raises the question whether the first excited state should be considered delocalized over the two cyclometalating ligands or localized on one of them. The analogous question for [Ru(bpy)$_3$]$^{2+}$ is still under intensive debate.[3,4]

Here we report results on several mixed-ligand chelate complexes of Rh^{3+}. Two of their three bidentate ligands are of the cyclometalating type, either 2-phenylpyridine anion (phpy$^-$) or 2-thienylpyridine anion (thpy$^-$), and the third ligand is either ethylenediamine (en) or 2,2'-bipyridine (bpy).[5-16] The complexes and their respective abbreviations, which will be used in the following, are listed in Table I.

* Author to whom correspondence should be addressed.
† Institut für Anorganische, Analytische und Physikalische Chemie.
‡ Laboratorium für Kristallographie.

(1) Kirch, M.; Lehn, J.-M.; Sauvage, J.-P.; *Helv. Chim. Acta* **1979**, *62*, 1345.
(2) Juris, A.; Balzani, V.; Barigelletti, F.; Campagna, S.; Belser, P.; von Zelewsky, A. *Coord. Chem. Rev.* **1988**, *84*, 85.
(3) Krausz, E.; Ferguson, J. *Prog. Inorg. Chem.* **1989**, *37*, 293.
(4) Yersin, H.; Braun, D.; Hensler, G.; Gallhuber, E. In *Vibronic Processes in Inorganic Chemistry*; Flint, C. D., Ed.; Kluwer Academic Publishers: Dordrecht, The Netherlands, 1989; pp 195–219.
(5) Zilian, A.; Mäder, U.; von Zelewsky, A.; Güdel, H. U. *J. Am. Chem. Soc.* **1989**, *111*, 3855.
(6) Zilian, A.; Colombo, M. G.; Güdel, H. U. *J. Lumin.* **1990**, *45*, 111.
(7) Colombo, M. G.; Zilian, A.; Güdel, H. U. *J. Am. Chem. Soc.* **1990**, *112*, 4581.
(8) Colombo, M. G.; Zilian, A.; Güdel, H. U. *J. Lumin.* **1991**, *48*, *49*, 549.
(9) Maestri, M.; Sandrini, D.; Balzani, V.; Mäder, U.; von Zelewsky, A. *Inorg. Chem.* **1987**, *26*, 1323.
(10) Ohsawa, Y.; Sprouse, S.; King, K. A.; DeArmond, M. K.; Hanck, K. W.; Watts, R. J. *J. Phys. Chem.* **1987**, *91*, 1047.
(11) Sandrini, D.; Maestri, M.; Balzani, V.; Mäder, U.; von Zelewsky, A. *Inorg. Chem.* **1988**, *27*, 2640.
(12) Riesen, H.; Krausz, E.; Zilian, A.; Güdel, H. U. *Chem. Phys. Lett.* **1991**, *182*, 271.
(13) Zilian, A.; Güdel, H. U. *Coord. Chem. Rev.* **1991**, *111*, 33.
(14) Zilian, A.; Güdel, H. U. *J. Lumin.* **1992**, *51*, 237.
(15) Giesbergen, C. P. M.; Sitters, R.; Frei, G.; Zilian, A.; Güdel, H. U.; Glasbeek, M. *Chem. Phys. Lett.* **1992**, *197*, 451.
(16) Zilian, A.; Güdel, H. U. *Inorg. Chem.* **1992**, *31*, 830.

0020-1669/92/1331-4766$03.00/0

Table I. Abbreviations Used for the Rh^{3+} Complexes

abbreviation	complex
PPB^+	[Rh(2-phenylpyridine)$_2$(2,2′-bipyridine)]$^+$
PPE^+	[Rh(2-phenylpyridine)$_2$(ethylenediamine)]$^+$
TTB^+	[Rh(2-thienylpyridine)$_2$(2,2′-bipyridine)]$^+$
TTE^+	[Rh(2-thienylpyridine)$_2$(ethylenediamine)]$^+$
TPB^+ or PTB^+	[Rh(2-thienylpyridine)(2-phenylpyridine)-(2,2′-bipyridine)]$^+$

Table II. Crystallographic Data for [PBB]PF_6

formula	$C_{32}H_{24}F_6N_4PRh$	temp (K)	100
fw	712.4	radiation (λ (Å))	Mo Kα (0.710 73)
cryst system	orthorhombic		
space group	*Pbca* (No. 61)	μ(Mo Kα) (cm^{-1})	6.75
a (Å)	10.821 (1)	d_{calc} (g/cm^3) (100 K)	1.661
b (Å)	15.798 (1)	d_{obs} (g/cm^3) (295 K)	1.6 (pycnometric method)
c (Å)	33.328 (3)		
V (Å^3)	5697.4 (9)	R^a	0.0254
Z	8	R_w^b	0.0336

^{a} $R = \Sigma||F_o| - |F_c||/\Sigma|F_o|$. ^{b} $R_w = [\Sigma w(|F_o| - |F_c|)^2/\Sigma wF_o^2]^{1/2}$.

2. Experimental Section

A. Synthesis and Crystallization. [PPB]PF_6 and [TTB]PF_6 were synthesized as described by Mäder et al.[17,18] For [PPB]BPh_4, [PPE]-PF_6, and [PPE]BPh_4 their method was adapted correspondingly. Single crystals suitable for crystal structure determination and optical absorption spectroscopy were obtained from slow diffusion of diethyl ether into a methanol solution of [PPB]PF_6 and [PPE]PF_6, respectively. [PPB]BPh_4 and [PPE]BPh_4 were recrystallized by the same method from a 2:1 dichloromethane/hexane (v/v) and a 5:1 acetone/hexane solution (v/v), respectively, by slow addition of hexane. ^{1}H-NMR spectra of [PPB]-BPh_4 showed that the recrystallized compound contains 1.5 molecules of dichloromethane per complex cation. The crystals have to be kept under a dichloromethane atmosphere to prevent them from becoming turbid due to loss of incorporated solvent molecules.

[TPB]PF_6 was synthesized using a 1:1 mixture of thpyH and phpyH and a procedure analogous to that of the above compounds. The product was shown to contain approximately 25% TTB^+, 50% TPB^+, and 25% PPB^+ by ^{1}H-NMR spectroscopy. No effort was made to separate TPB^+ from this mixture because many of the spectroscopic properties of this compound can be investigated by doping [PPB]PF_6 with 1% of the mixture. This gives crystals which contain approximately 0.25% TTB^+ and 0.5% TPB^+. To get [PPB]PF_6 crystals doped with 1% TPB^+ only, [PPB]PF_6 was synthesized starting with a 200:1 mixture of phpyH and thpyH, thus reducing the TTB^+ content to approximately 0.01%. [PPB]PF_6 doped with 1% TTB^+ was obtained by recrystallization of [PPB]PF_6 with the appropriate amount of [TTB]PF_6.

B. Structure Determination. [PPB]PF_6 crystallizes as yellow needles. A single crystal with dimensions 0.15 mm × 0.24 mm × 0.22 mm was used for data collection with an Enraf-Nonius CAD4 diffractometer at 100 K (Mo Kα radiation, λ = 0.710 73 Å, graphite monochromator). A total of 7614 reflections were collected in the range $0° \le 2\theta \le 56°$, with $0 \le h \le 14$, $0 \le k \le 20$, and $0 \le l \le 44$, in the ω-scan technique. Absorption effects were corrected via the empirical method based on ψ-scans (EAC program of the Structure Determination Package from Enraf-Nonius; minimum correction 0.978, maximum correction 1.000). For structure solution and refinement 4556 unique reflections with $I \ge 3\sigma(I)$ were used. The structure was solved by direct methods (programs SHELX76 and SHELXS86). Anisotropical non-hydrogen atoms and isotropic H atoms were refined. Real and imaginary scattering factors were taken from ref 19, and no extinction correction was applied. Final $R = 0.0254$, and final $R_w = 0.0336$. Crystallographic data are given in Table II. Bond lengths and angles, thermal parameters, and detailed information concerning data collection and processing are available as supplementary material.

C. Absorption Spectroscopy. Single-crystal absorption spectra were measured with a double-beam attachment built in this laboratory, using a 100-W halogen lamp, a 1401 or a 1402 Spex double monochromator with two gratings (1200 grooves/mm) blazed at 500 nm, a Glan–Taylor polarizing prism, microoptics, and an EMI 9781A PM tube. The crystals were mounted on aluminum plates with a small hole or slit and cooled in a double-walled helium-gas flow tube.[20] The [PPB]PF_6 crystals, whose dimensions were approximately 0.1 mm × 0.4 mm × 0.6 mm and 0.2 mm × 0.2 mm × 3 mm, respectively, were oriented with the help of precession photographs. One crystal was used to measure the absorption spectra along *c* with the electric field vector polarized parallel to the crystal *a* and *b* axes, respectively. For polarization of the electric field vector parallel to the *b* and *c* axes another crystal was used with the light propagation vector parallel to the *a* axis. [PPB]BPh_4, [PPE]PF_6, and [PPE]BPh_4 crystals were mounted under the microscope between crossed Nicols so that the absorption spectra could be measured with the electric field vector parallel to the extinction directions of the crystals.

D. Luminescence and Excitation Spectroscopy. For luminescence spectra polycrystalline samples were sealed in glass capillaries and cooled in a double-walled helium-gas flow tube.[20] Lines of a Spectra Physics 2045 Ar^+ laser or a Lambda Physik FL3001/2 dye laser with a methanol solution of Coumarin 152 pumped by a Quanta-Ray DCR-3 Nd:YAG laser were used for excitation. The luminescence was dispersed by a Spex 1402 double monochromator with two gratings blazed at 500 nm (1200 grooves/mm) or a Spex 1702 $^3/_4$-m monochromator with a grating blazed at 300 nm (1200 grooves/mm) and detected by a cooled RCA C31034 photomultiplier and a photon-counting system (Stanford Research SR 400). A Tektronix 4052A microcomputer was used for monochromator and dye laser control and for data acquisition.

Polarized single-crystal excitation spectra of TTB^+ doped into [PPB]-PF_6 were measured with the same apparatus as the absorption spectra. The luminescence of TTB^+ was detected at a right angle to the exciting light by a cooled Hamamatsu R3310-01 PM and a photon-counting system (Stanford Research SR 400) after passing through a cut-off filter (Schott OG550) below 18 200 cm^{-1}. The crystal was mounted on a fiber and cooled in a double-walled flow tube.[20] The same polarizations of the electric field vector were used for excitation as for the polarized single-crystal absorption spectra of the [PPB]PF_6 host.

3. Results

A. Crystal and Molecular Structure of [PPB]PF_6. There is only one complex cation per asymmetric unit lying in general position; i.e., at 100 K all eight Rh atoms in the unit cell are crystallographically equivalent. The same is true for the eight bpy ligands. There are two $phpy^-$ ligands per Rh, however, and these are crystallographically inequivalent; i.e. as far as $phpy^-$ alone is concerned, there are two different sites. Bond lengths and bond angles related by the approximate molecular 2-fold axis do not show significant differences in the two different $phpy^-$ ligands, but some of the corresponding C–Rh–N and N–Rh–N angles do (e.g. C1–Rh–N3 = 96.4 (1)° and C6–Rh–N4 = 100.7 (1)°). Thus the molecular 2-fold symmetry axis of PPB^+ is not exactly maintained in the crystal. Figure 1 shows the molecular structure of the PPB^+ complex and the numbering scheme adopted (hydrogen atoms are omitted for clarity; their labels correspond to those of the carbon atoms to which they are attached). Atomic positional parameters are given in Table III.

B. Single-Crystal Absorption and Excitation Spectroscopy. Figure 2 shows the low-temperature single-crystal absorption spectra of [PPB]PF_6 in the region of the first excited states for polarization of the electric field vector parallel to the crystal *a*, *b*, and *c* axes, respectively. The spectra were measured with two different crystals. The *b*-polarized spectrum could be measured for both crystals and was used for scaling. It is impressive how highly structured these spectra are in comparison to the commonly measured solution spectra, which at room temperature show no absorption bands in this region. It was shown in an earlier publication that nearly all the lines in the *a*- and *b*-polarized spectra can be interpreted as vibrational sidebands of the two electronic origin lines labeled C and D.[5] In ref 5 two additional weak lines A and B were reported. As shown in detail in ref 16,

(17) Mäder, U. Cyclometallierte Rhodium(III)-Komplexe. Inaugural-Dissertation, Universität Freiburg, Freiburg, Switzerland, 1987 (Diss. No. 933).
(18) Mäder, U.; Jenni, T.; von Zelewsky, A. *Helv. Chim. Acta* **1986**, *69*, 1085.
(19) International Union of Crystallography: *International Tables for X-Ray Crystallography*; Kynoch Press: Birmingham, England, 1974; Vol. IV, Table 2.2B, pp 90–101, Table 2.3.1, pp 149–150.
(20) Krausz, E.; Tomkins, C.; Adler, H. *J. Phys. E: Sci. Instrum.* **1982**, *15*, 1167.

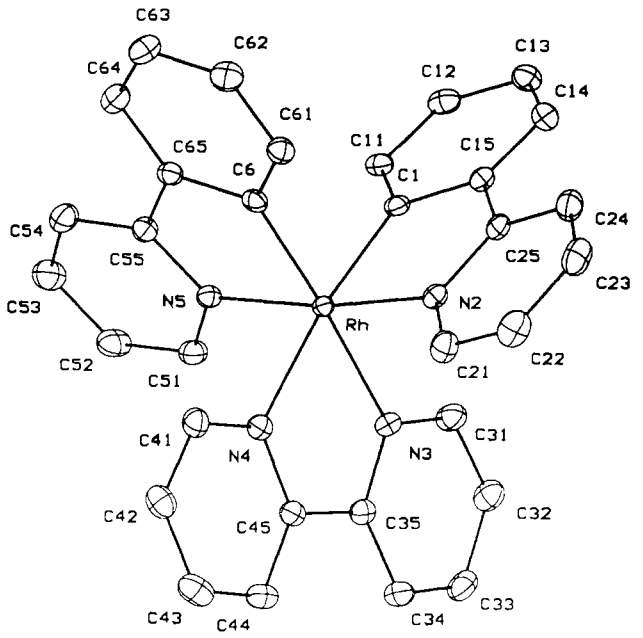

Figure 1. Molecular structure of the PPB^+ complex in $[PPB]PF_6$, showing atomic numbering scheme and anisotropic rms displacements (×1.54) produced by the program PEANUT.[21] Note that these are not the conventional equiprobability ellipsoids. Hydrogen atoms are omitted for clarity.

they are due to impurities. The assignment is shown at the top of Figure 2. The *c*-polarized spectrum shows several new lines which have not been noticed before because they are much weaker for the other two polarizations. The new lines can be interpreted as vibrational sidebands of a third electronic origin line labeled N. Although the vibrational sidebands of line N are similar to the ones of C and D, there are significant differences, as shown in Table IV. Table V shows the relative intensities of the three origin absorption lines C, D, and N for the different polarizations. Polarized excitation spectra of TTB^+-doped $[PPB]PF_6$ show the C and D lines of TTB^+ at 19 204 and 19 360 cm^{-1}, respectively.[16] They are separated by 156 cm^{-1} and have roughly the same polarization ratios as the pure host. It appears, therefore, that the chemical bonding in the PPB^+ and TTB^+ complexes is similar, and the analysis presented in section 4.D for PPB^+ also applies to TTB^+.

The single-crystal absorption spectra of $[PPB]BPh_4$, $[PPE]PF_6$, and $[PPE]BPh_4$ are very similar to those of $[PPB]PF_6$, as far as the general pattern of the origin lines and the vibrational sidebands are concerned. However, they do show several important differences. The origin line N can be observed in $[PPB]BPh_4$ but not in $[PPE]PF_6$ and $[PPE]BPh_4$. As for $[PPB]PF_6$ the polarization properties of the line N and its sidebands are different from those of the lines C and D also for $[PPB]BPh_4$. C and D, on the other hand, have very similar polarization ratios in both compounds; cf. Figure 3.

The energy difference between the two origin lines C and D varies from 22 cm^{-1} in $[PPB]PF_6$ up to 242 cm^{-1} in $[PPE]BPh_4$ (see Table VI), whereas the intensities of the two lines are comparable in all the compounds; see Figure 3. Because of the large energetic C–D splitting in $[PPE]PF_6$ and $[PPE]BPh_4$, the high-energy wings of the origin lines are clearly resolved for these compounds. They result from coupling of the electronic transition to lattice modes or phonons. Figure 3 shows a great variation of the relative intensity of these phonon wings.

As for $[PPB]PF_6$, the vibrational sideband energies relative to origin line C are the same as the corresponding energies relative to D for both $[PPE]PF_6$ and $[PPB]BPh_4$. For $[PPE]BPh_4$,

(21) Hummel, W.; Hauser, J.; Bürgi, H.-B. *J. Mol. Graphics* **1990**, *8*, 214.

Table III. Atomic Positional Parameters and Isotropic Equivalent Displacement Parameters of $[PPB]PF_6$[a]

	x/a	*y/b*	*z/c*	B_{eq}[b] (Å²)
Rh	0.23614 (1)	0.75164 (1)	0.13891 (1)	0.742 (3)
P	−0.22763 (6)	0.85985 (4)	0.05390 (2)	1.33 (1)
F1	−0.3578 (1)	0.8135 (1)	0.0570 (1)	2.32 (3)
F2	−0.1875 (2)	0.7996 (1)	0.0179 (1)	2.38 (3)
F3	−0.2855 (2)	0.9253 (1)	0.0224 (1)	2.88 (4)
F4	−0.0976 (2)	0.9076 (1)	0.0513 (1)	3.11 (4)
F5	−0.2665 (2)	0.9220 (1)	0.0899 (1)	2.42 (3)
F6	−0.1702 (2)	0.7954 (1)	0.0856 (1)	2.85 (3)
C1	0.3622 (2)	0.8275 (1)	0.1633 (1)	0.89 (4)
C11	0.3443 (2)	0.9029 (2)	0.1840 (1)	1.08 (4)
C12	0.4438 (2)	0.9528 (2)	0.1957 (1)	1.28 (4)
C13	0.5643 (2)	0.9282 (2)	0.1868 (1)	1.38 (4)
C14	0.5851 (2)	0.8528 (2)	0.1667 (1)	1.37 (4)
C15	0.4857 (2)	0.8028 (2)	0.1551 (1)	0.98 (4)
C25	0.4994 (2)	0.7241 (2)	0.1320 (1)	1.01 (4)
C24	0.6103 (3)	0.6827 (2)	0.1241 (1)	1.46 (4)
C23	0.6094 (3)	0.6089 (2)	0.1016 (1)	1.63 (4)
C22	0.4989 (3)	0.5789 (2)	0.0870 (1)	1.71 (5)
C21	0.3918 (3)	0.6219 (2)	0.0957 (1)	1.47 (4)
N2	0.3909 (2)	0.6925 (1)	0.1183 (1)	0.96 (3)
N3	0.2187 (2)	0.8192 (1)	0.0835 (1)	1.02 (3)
C31	0.2745 (3)	0.8932 (2)	0.0754 (1)	1.41 (4)
C32	0.2583 (3)	0.9351 (2)	0.0397 (1)	1.51 (4)
C33	0.1819 (2)	0.8998 (2)	0.0109 (1)	1.47 (4)
C34	0.1259 (2)	0.8228 (2)	0.0186 (1)	1.38 (4)
C35	0.1457 (2)	0.7835 (2)	0.0552 (1)	1.04 (4)
C45	0.0870 (2)	0.7025 (2)	0.0667 (1)	1.02 (4)
C44	0.0144 (2)	0.6546 (2)	0.0409 (1)	1.41 (4)
C43	−0.0375 (2)	0.5800 (2)	0.0547 (1)	1.69 (5)
C42	−0.0164 (2)	0.5542 (2)	0.0938 (1)	1.50 (4)
C41	0.0582 (2)	0.6039 (2)	0.1176 (1)	1.37 (4)
N4	0.1095 (2)	0.6763 (1)	0.1047 (1)	1.04 (3)
N5	0.0904 (2)	0.8078 (1)	0.1673 (1)	0.94 (3)
C51	0.0186 (2)	0.8687 (2)	0.1514 (1)	1.27 (4)
C52	−0.0798 (2)	0.9034 (2)	0.1720 (1)	1.54 (4)
C53	−0.1062 (3)	0.8744 (2)	0.2100 (1)	1.71 (5)
C54	−0.0340 (2)	0.8107 (2)	0.2265 (1)	1.50 (4)
C55	0.0653 (2)	0.7782 (2)	0.2047 (1)	1.11 (4)
C65	0.1497 (2)	0.7114 (2)	0.2184 (1)	1.02 (4)
C64	0.1429 (2)	0.6746 (2)	0.2564 (1)	1.43 (4)
C63	0.2267 (3)	0.6119 (2)	0.2671 (1)	1.53 (5)
C62	0.3152 (3)	0.5859 (2)	0.2395 (1)	1.47 (4)
C61	0.3218 (2)	0.6223 (2)	0.2018 (1)	1.22 (4)
C6	0.2407 (2)	0.6867 (2)	0.1902 (1)	0.94 (4)
H11	0.259 (2)	0.923 (2)	0.1900 (8)	0.9 (2)*
H12	0.428 (3)	1.005 (2)	0.2078 (9)	1.9 (3)*
H13	0.631 (3)	0.959 (2)	0.1950 (9)	1.8 (3)*
H14	0.666 (3)	0.835 (2)	0.1623 (8)	1.5 (2)*
H24	0.683 (3)	0.701 (2)	0.1356 (9)	1.5 (2)*
H23	0.678 (3)	0.579 (2)	0.0966 (9)	1.8 (3)*
H22	0.494 (3)	0.530 (2)	0.0719 (9)	1.9 (3)*
H21	0.317 (3)	0.602 (2)	0.0860 (8)	0.9 (2)*
H31	0.322 (2)	0.917 (2)	0.0961 (8)	0.9 (2)*
H32	0.297 (3)	0.987 (2)	0.036 (1)	1.9 (3)*
H33	0.169 (3)	0.927 (2)	−0.0134 (9)	1.8 (3)*
H34	0.078 (3)	0.799 (2)	−0.0005 (9)	1.5 (2)*
H44	0.004 (3)	0.673 (2)	0.0149 (9)	1.5 (2)*
H43	−0.085 (3)	0.545 (2)	0.0371 (9)	1.8 (3)*
H42	−0.046 (3)	0.505 (2)	0.1056 (9)	1.9 (3)*
H41	0.078 (2)	0.591 (2)	0.1431 (8)	0.9 (2)*
H51	0.038 (2)	0.884 (2)	0.1255 (9)	0.9 (2)*
H52	−0.123 (3)	0.944 (2)	0.1588 (9)	1.9 (3)*
H53	−0.179 (3)	0.895 (2)	0.2265 (9)	1.8 (3)*
H54	−0.052 (3)	0.788 (2)	0.2524 (9)	1.5 (2)*
H64	0.081 (3)	0.693 (2)	0.2771 (8)	1.5 (2)*
H63	0.221 (3)	0.590 (2)	0.2921 (9)	1.8 (3)*
H62	0.363 (3)	0.546 (2)	0.2464 (9)	1.9 (3)*
H61	0.385 (2)	0.603 (2)	0.1840 (8)	0.9 (2)*

[a] The atoms are numbered as shown in Figure 1. Hydrogen atoms are numbered as the carbon atoms to which they are bonded. [b] Starred *B* values are for atoms that were refined isotropically. Anisotropically refined atoms are given in the form of the isotropic equivalent displacement parameter B_{eq}. Definitions:[22,23] $B_{eq} = {}^8/_3\pi^2 \sum_i(\sum_j(U_{ij}a_i^*a_j^*\bar{a}_i\bar{a}_j))$. $\sigma_{B_{eq}} = {}^8/_3\pi^2\{(\sigma_{U_{11}}{}^2 + \sigma_{U_{22}}{}^2 + \sigma_{U_{33}}{}^2)[1 - (U_{11}U_{22} + U_{11}U_{33} + U_{22}U_{33})/2(U_{11}{}^2 + U_{22}{}^2 + U_{33}{}^2)]\}^{1/2}$.

(22) Hamilton, W. C. *Acta Crystallogr.* **1959**, *12*, 609.
(23) Schomaker, V.; Marsh, R. E. *Acta Crystallogr.* **1983**, *A39*, 819.

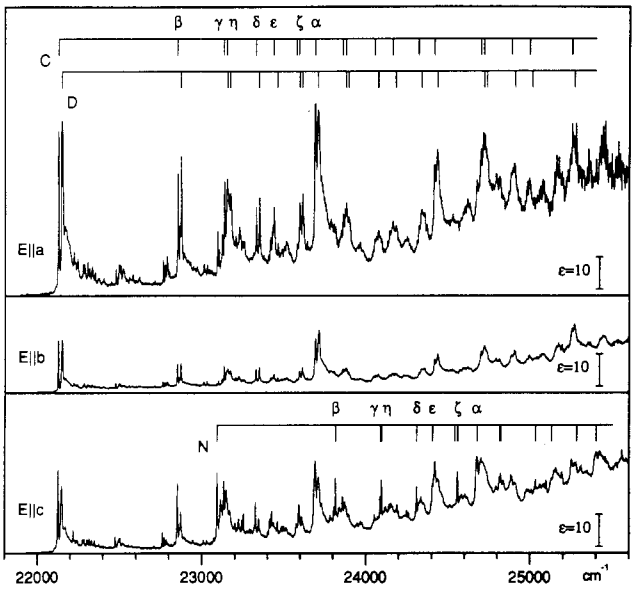

Figure 2. Single-crystal absorption spectra of [PPB]PF$_6$ at 10 K with the electric vector polarized parallel to the crystal *a*, *b*, and *c* axes. Electronic origins are labeled C, D, and N, respectively. Vibrational sidebands are labeled according to Table IV (α, β, γ, ...); combination bands, however, are not labeled.

Table IV. Vibrational Sideband Energies (in cm^{-1}) Relative to the Origin Lines C, D, and N[a]

	β	γ	η	δ	ϵ	ζ	α
[PPB]PF$_6$ (C)	726	1009	1027	1202	1311	1468	1566
[PPB]BPh$_4$ (C)	733	1009	1029	1201	1301		1567
[PPE]PF$_6$ (C)	728	1014	1026	1184	1294	1464	1550
[PPE]BPh$_4$ (C)	720	1007		1183		1465	1550
[PPE]BPh$_4$ (D)	737	1017		1209		1482	1568
[PPB]PF$_6$ (N)	724	996	1004	1218	1313	1466	1584
[PPB]BPh$_4$ (N)	720	991					

[a] Only the values for the transition C are listed if there are no significant differences between C and D. The vibrations are designated as in ref 5 with the exception of η and ζ, which have not been assigned previously.

Table V. Relative Intensities (Arbitrary Units) of Absorption Lines C, D, and N in [PPB]PF$_6$ Measured for Three Polarization Directions of the Electric Field Vector *E*[a]

	line C	line D	line N
$E\|\|a$	0.850	0.777	0.171
$E\|\|b$	0.161	0.141	0.009
$E\|\|c$	0.522	0.188	0.315

[a] See Figure 2.

however, which has the greatest energetic splitting of the origin lines C and D, the corresponding vibrations are significantly different; see Table IV.

C. Luminescence Spectroscopy of Doped Systems. Figure 4 shows the highly structured luminescence spectra of [PPB]PF$_6$ doped with 0.25% TTB$^+$ and 0.5% TPB$^+$ for different excitation: The Ar$^+$ line at 514.5 nm (19 430 cm^{-1}) is exciting only the dopant complexes TTB$^+$ and TPB$^+$ because the host lattice shows no absorption below 22 100 cm^{-1} (Figure 2). The three origin lines at 19 204, 19 233, and 19 307 cm^{-1} with their vibrational sidebands at lower energy must therefore be due to these dopant complexes. The origin region is enlarged in Figure 5, and the three lines are designated X, Y, and Z, respectively. The Ar$^+$ line at 363.8 nm (27 480 cm^{-1}), on the other hand, excites a relatively strong metal-to-ligand charge-transfer (MLCT) transition of the host lattice. The dopant complexes are thus mainly excited via nonradiative energy transfer from the host complexes (host-sensitized luminescence).[16] That is why the relative intensities of the three origin lines are different in the spectra of

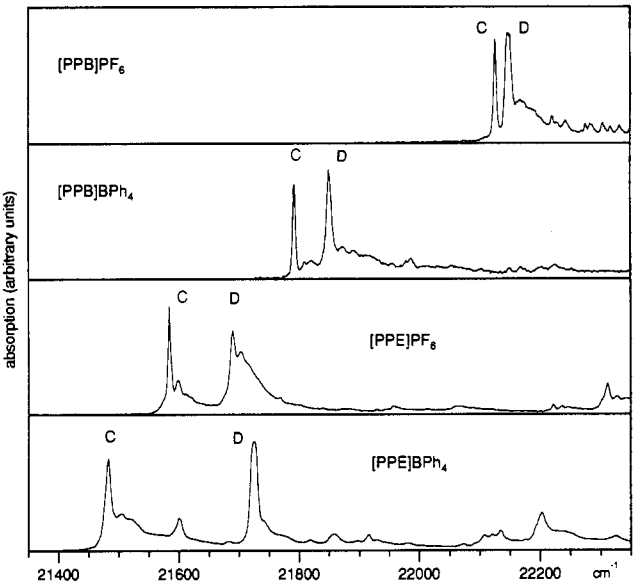

Figure 3. Single-crystal absorption spectra of [PPB]PF$_6$, [PPB]BPh$_4$, [PPE]PF$_6$, and [PPE]BPh$_4$ at 10 K in the region of the first electronic origins C and D.

Table VI. Energy of the Origin Lines C, D, and N and Energetic Splitting between C, D, and N (in cm^{-1}) for [PPB]PF$_6$, [PPB]BPh$_4$, [PPE]PF$_6$, and [PPE]BPh$_4$[a]

	line C	line D	line N	Δ(C–D)	Δ(C–N)
[PPB]PF$_6$	22 126	22 148	23 093	22	967
[PPB]BPh$_4$	21 793	21 851	22 911	58	1118
[PPE]PF$_6$	21 584	21 690		106	
[PPE]BPh$_4$	21 483	21 725		242	

[a] See Figure 3.

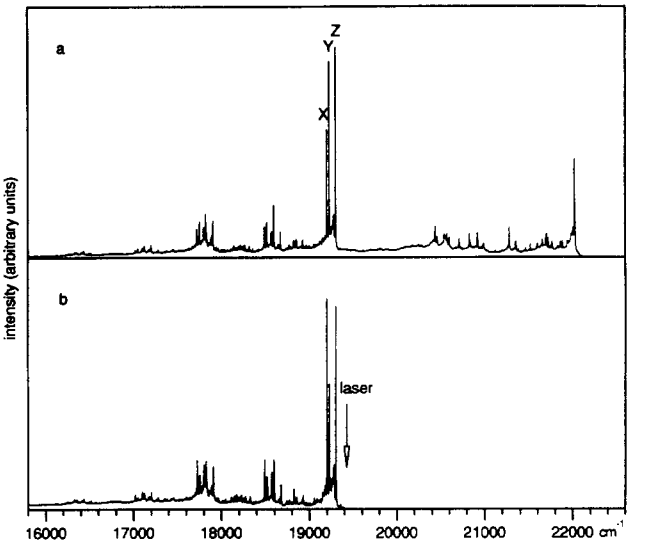

Figure 4. 7 K luminescence spectra of [PPB]PF$_6$ doped with 0.25% TTB$^+$ and 0.5% TPB$^+$ excited with the Ar$^+$ laser at (a) 363.8 nm (27 480 cm^{-1}) and (b) 514.5 nm (19 430 cm^{-1}). The origins X, Y, and Z are discussed in the text and shown in more detail in Figure 5a.

Figure 4a,b. The energy-transfer properties of this lattice have been discussed in another paper.[16]

The 19 204-cm^{-1} origin line of the dopant complexes can also be observed for [PPB]PF$_6$ doped with 1% TTB$^+$;[16] see Figure 5b, line X. It coincides exactly with the lowest-energy absorption line C of TTB$^+$ doped into [PPB]PF$_6$, as determined by excitation spectra; see section 3.B. [PPB]PF$_6$ doped wtih 1% TPB$^+$, on the other hand, shows the other two origin lines Y and Z at 19 233 and 19 307 cm^{-1}, as is illustrated in the Figure 5c.

Luminescence spectra for selective excitation of the three origin lines X, Y, and Z are shown in Figure 6. Although the vibrational

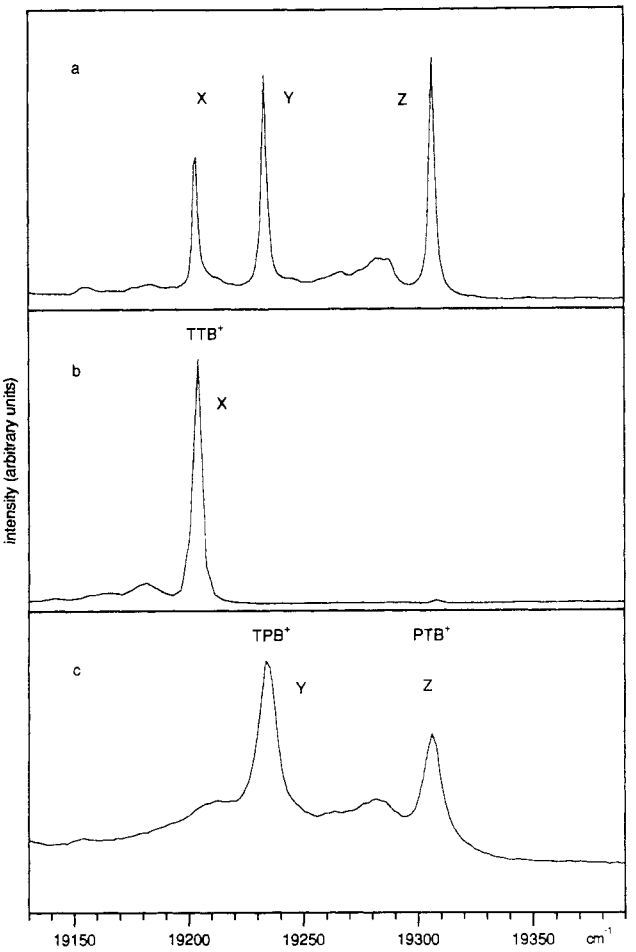

Figure 5. Origin regions of 7 K luminescence spectra for (a) 0.25% TTB^+ and 0.5% TPB^+ (cf. Figure 4a), (b) 1% TTB^+ (from ref 16), and (c) 1% TPB^+, all doped into $[PPB]PF_6$ and excited at 363.8 nm (27 480 cm^{-1}).

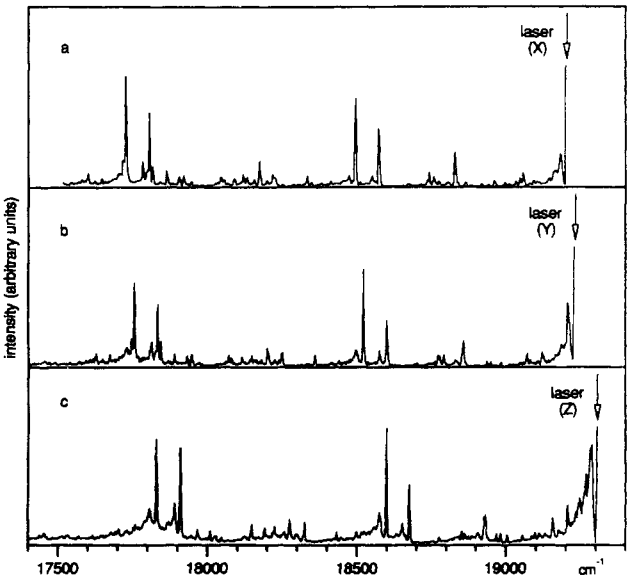

Figure 6. Selectively excited luminescence spectra at 7 K of 0.25% TTB^+ and 0.5% TPB^+ doped into $[PPB]PF_6$. Excitations are at (a) 19 204 cm^{-1} (position of line X in Figure 5), (b) 19 233 cm^{-1} (position of line Y in Figure 5), and (c) 19 307 cm^{-1} (position of line Z in Figure 5). The spectra start approximately 3 cm^{-1} below the position of the laser line. The peak maxima of the origin lines are therefore not shown.

sideband patterns are very similar for the three spectra, with energy differences of less than 5 cm^{-1} for the most prominent sidebands, the three spectra differ in their absolute energetic positions, thus identifying the three lines X, Y, and Z as being due to three different luminescent species in the crystal. The luminescence spectra of Figure 4, which consist of a superposition of three very similar spectra, can thus be decomposed into their components by site-selective laser spectroscopy.

4. Discussion

A. Structural Considerations. The structure determination of $[PPB]PF_6$ confirms the cis arrangement of the two cyclometalating carbon atoms in the $phpy^-$ ligands. The two nitrogen atoms of bpy are trans to these carbon atoms as was already concluded from NMR spectroscopy.[18] There are three types of Rh–ligand bonds for $[PPB]PF_6$ which show significantly different lengths: The average value of the Rh–C distances is 1.992 (3) Å, and the average Rh–N distances are 2.039 (2) and 2.142 (2) Å for the $phpy^-$ and the bpy ligands, respectively. The significant difference between the Rh–N($phpy^-$) and the Rh–N(bpy) distances indicates a strong trans influence of the Rh–C bonds on the Rh–N(bpy) bonds.

Important bond distances of $[PPB]PF_6$ and of similar compounds[24-33] are compared in Table VII. Metal–carbon distances are typically 1.99 Å and therefore shorter than metal–nitrogen distances, which are about 2.04 Å for compounds in which the metal ion is coordinated by nitrogen atoms only. Due to the trans influence of the cyclometalating carbon atoms, metal–nitrogen bonds trans to these carbon atoms are weakened and therefore consistently longer (2.14 Å) than metal–nitrogen bonds in a cis position to a metal–carbon bond, which are about 2.04 Å. Trans influence has not been observed for the closely related complex $[Rh(phpy)(bpy)_2](PF_6)_2$[25] because this compound shows a 6-fold crystallographic disorder associated with the phenyl and pyridyl rings, which only allows the determination of a mean metal–ligand bond length. In ref 25 it was assumed that all the Rh–ligand bond lengths are equal, and it was concluded that the replacement of a bpy ligand of $[Rh(bpy)_3]^{3+}$ by the isostructural and isoelectronic cyclometalating $phpy^-$ ligand has no significant effect upon the structure of the complex ion. This conclusion contradicts the results of the structure determinations of the other compounds listed in Table VII. On the basis of our results, the following bond lengths would be expected for the $[Rh(phpy)(bpy)_2]^{2+}$ cation: 1.99 Å for the Rh–C bond, 2.14 Å for the Rh–N bond trans to the cyclometalating carbon atom, and 2.04 Å for the four other Rh–N bonds. This non-equal-length model agrees well with the structural parameters of $[Ir(bpy\text{-}C,N')(bpy\text{-}N,N')_2]^{2+}$,[30] where the metal ion is also coordinated to one carbon and five nitrogen atoms. The mean bond length for such a complex in a 6-fold-disordered structure would be 2.048 (20) Å, which is compatible with the value of 2.043 (3) Å reported in ref 25 for the $[Rh(phpy)(bpy)_2](PF_6)_2$ structure.

A detailed analysis of the displacement parameters of $[Rh(phpy)(bpy)_2](PF_6)_2$ (taken from the supplementary material to ref 25) along the lines described in refs 34 and 35 shows that these parameters are also compatible with the non-equal-length

(24) Hubesch, B.; Mahieu, B.; Meunier-Piret, J. *Bull. Soc. Chim. Belg.* **1985**, *94*, 685.
(25) Constable, E. C.; Leese, T. A.; Tocher, D. A. *Polyhedron* **1990**, *9*, 1613.
(26) Mäder, U.; Stöckli-Evans, H.; von Zelewski, A. Personal communication.
(27) Rillema, D. P.; Jones, D. S.; Levy, H. A. *J. Chem. Soc., Chem. Commun.* **1979**, 849.
(28) Reveco, P.; Schmehl, R. H.; Cherry, W. R.; Fronczek, F. R.; Selbin, J. *Inorg. Chem.* **1985**, *24*, 4078.
(29) Hazell, A. C.; Hazell, R. G. *Acta Crystallogr.* **1984**, *C40*, 806.
(30) Nord, G.; Hazell, A. C.; Hazell, R. G.; Farver, O. *Inorg. Chem.* **1983**, *22*, 3429.
(31) Hazell, A.; Simonsen, O.; Wernberg, O. *Acta Crystallogr.* **1986**, *C42*, 1707.
(32) Chassot, L.; Müller, E.; von Zelewski, A. *Inorg. Chem.* **1984**, *23*, 4249.
(33) Deuschel-Cornioley, Ch.; Stöckli-Evans, H.; von Zelewski, A. *J. Chem. Soc., Chem. Commun.* **1990**, 121.
(34) Chandrasekhar, K.; Bürgi, H.-B. *Acta Crystallogr.* **1984**, *B40*, 387.
(35) Stebler, M.; Ludi, A.; Bürgi, H.-B. *Inorg. Chem.* **1986**, *25*, 4743.

Table VII. Comparison of M–C and M–N Bond Lengths (Å) in [PPB]PF$_6$ and Related Complexes

substance	coord sphere	M–C	M–N(cis)	M–N(trans)	ref
[Rh(bpy)$_3$]Cl$_3$	RhN_6		2.036 (1)[a]		24
[Rh(phpy)(bpy)$_2$](PF$_6$)$_2$	RhN_5C		2.043 (3)[b]		25
[Rh(phpy)$_2$(bpy)]PF$_6$	RhN_4C_2	1.992 (3)[a]	2.039 (2)[a]	2.142 (2)[a]	
[Rh(thpy)$_2$(bpy)]Cl·2$^1/_8$H$_2$O	RhN_4C_2	1.989 (5)[a]	2.060 (5)[a]	2.142 (4)[a]	26
[Ru(bpy)$_3$](PF$_6$)$_2$	RuN_6		2.056 (6)		27
[Ru(bpy)$_2$(4-nitro-phpy)]BF$_4$	RuN_5C	1.997 (7)	2.064 (10)[a]	2.140 (5)	28
[Ir(bpy)$_3$](ClO$_4$)$_3$·2$^1/_3$H$_2$O	IrN_6		2.021 (5)[a]		29
[Ir(bpy)$_2$(bpy-*C*,*N*')](ClO$_4$)$_2$·$^1/_3$H$_2$O	IrN_5C	1.980 (6)	2.054 (5)[a]	2.131 (5)	30
[Pt(bpy)$_2$](NO$_3$)$_2$·H$_2$O	PtN_4		2.027 (2)[a]		31
[Pt(phpy)$_2$]	PtN_2C_2	1.988 (9)[a]		2.127 (2)[a]	32
[Pt(diphpy)$_2$][c]	PtN_2C_2	1.987 (22)[a]		2.158 (6)[a]	33

[a] Mean values with their estimated standard deviations, $\sigma_{\langle d\rangle} = \{[\sum(d_i - \langle d\rangle)^2]/[m(m-1)]\}^{1/2}$, in parentheses. [b] For the disordered structure of [Rh(phpy)(bpy)$_2$](PF$_6$)$_2$,[25] only a mean value for the Rh–X distances can be derived from the experimental data. [c] diphpy$^-$ = 2,6-diphenylpyridine anion.

model derived from the [PPB]PF$_6$ structure: First the mean square displacement along the Rh–X bond vector of the metal ion is subtracted from that of the coordinating ligand atom to obtain the intramolecular parameter

$$\Delta U_{\text{intra(X-Rh)}} = U(\text{X})_{\text{X}\rightarrow\text{Rh}} - U(\text{Rh})_{\text{Rh}\rightarrow\text{X}} \quad (1)$$

$\Delta U_{\text{intra(X-Rh)}}$ depends only on the contribution from vibration (vib) and disorder within the complex and not on the translation and rotation of the complex as a whole:

$$\Delta U_{\text{intra(X-Rh)}} = \Delta U_{\text{vib}} + \Delta U_{\text{disorder}} \quad (2)$$

We assume that for the non-equal-length model the vibrational contribution ΔU_{vib} of disordered [Rh(phpy)(bpy)$_2$](PF$_6$)$_2$ can be approximated by the value of ΔU_{vib} for ordered [PPB]PF$_6$, which is simply the average of the six quantities $\Delta U_{\text{intra(X-Rh)}}$ (X = N, C):

$$\Delta U_{\text{vib}}(\text{model}) = \langle \Delta U_{\text{intra(X-Rh)}}([\text{PPB}]\text{PF}_6)\rangle = 0.0027\ (4)\ \text{Å}^2 \quad (3)$$

The $\Delta U_{\text{disorder}}$ contribution along the Rh–X bond vector may be estimated from the mean square deviation of individual Rh–X distances (in the non-equal-length model) from their mean value $\langle d\rangle$:

$$\Delta U_{\text{disorder}}(\text{model}) = {}^1/_6 \sum_{i=1}^{6}(d_i - \langle d\rangle)^2 = 0.002\ \text{Å}^2 \quad (4)$$

Using eq 2, the sum of the estimated vibrational and disorder contributions from eqs 3 and 4, respectively, gives $\Delta U_{\text{intra(X-Rh)}}(\text{model}) = 0.0047\ (4)$ Å^2 for the non-equal-length model. The corresponding value derived from the experimentally determined displacement parameters for the [Rh(phpy)(bpy)$_2$]-(PF$_6$)$_2$ structure using eq 1 is 0.0029 (14) Å^2. These two values are equal within the 2σ-range, indicating that the thermal parameters of [Rh(phpy)(bpy)$_2$](PF$_6$)$_2$ are not incompatible with the more reasonable non-equal-length model. We conclude that the Rh–C and Rh–N bond lengths of the [Rh(phpy)(bpy)$_2$]$^{2+}$ cation are unequal, as predicted by the non-equal-length model.

B. Number of Sites at 7 K. The crystal structure of [PPB]PF$_6$ shows that there is only one crystallographic site for the PPB$^+$ complex at 100 K (section 3.A). The spectroscopic evidence obtained between 7 and 20 K is consistent with the assumption that the crystal structure does not change between 100 and 7 K. Specifically, luminescence spectra of TTB$^+$ doped into [PPB]-PF$_6$ show only one origin line X at 19 204 cm^{-1} (Figure 5b), which is due to emission from the lowest excited state of TTB$^+$.[16] In contrast, luminescence spectra of TPB$^+$ doped into [PPB]PF$_6$ show two origin lines at 19 233 cm^{-1} (Y) and 19 307 cm^{-1} (Z) (Figure 5c), due to two different TPB$^+$ traps. The existence of two such traps follows directly from the crystal structure of the host material: When TPB$^+$ is doped into [PPB]PF$_6$, the bpy ligand of the dopant complex is likely to occupy the same position as the bpy ligand of the substituted PPB$^+$ complex. The thpy$^-$ ligand can occupy either one of the two crystallographically inequivalent phpy$^-$ sites of the host material, thus leading to two different sorts of traps denoted TPB$^+$ and PTB$^+$ in Figure 5. The luminescence spectra of doped [PPB]PF$_6$ crystals thus clearly show that in this compound there is one PPB$^+$ complex site with two inequivalent phpy$^-$ ligands down to 7 K. This is a nice demonstration that dilution of a complex by doping it into an appropriate host lattice can be used to study its intrinsic properties.

C. Assignment of the Observed Transitions. The question whether the lowest-energy excitations in PPB$^+$ and TTB$^+$ should be assigned to ligand-centered (LC) triplet $\pi \rightarrow \pi^*$ or to triplet MLCT transitions was discussed in refs 5, 7, 12, 13, and 14. On the basis of the absorption spectra, a triplet MLCT assignment was favored.[5] However, luminescence line narrowing and hole burning experiments[7,12] as well as Zeeman luminescence experiments[13,14] revealed a behavior of this excited state which is more typical of a triplet LC transition. Strong support of the latter assignment is provided by recent optically detected magnetic resonance (ODMR) experiments on TTB$^+$-doped [PPB]PF$_6$ crystals.[15] In addition, we have recently been able to observe both the triplet LC and the MLCT transitions in the absorption spectra of the analogous Ir^{3+} complexes. It appears that the two types of transition can retain their typical character even when closely approaching each other in energy. Both types of transition steal their intensity from singlet MLCT excitations. As far as intensity and its polarization is concerned, they can therefore not easily be distinguished. More important are excited-state g values, their zero-field splitting, and the band shapes observed in absorption and luminescence. For PPB$^+$ and TTB$^+$ these all favor a triplet LC assignment. The present paper cannot contribute a great deal to this question. All the conclusions reached here are in agreement with a triplet LC assignment.

It has already been discussed in ref 16 that the vibrational frequencies of the ground state of the TTB$^+$ complex are essentially unaffected by its environment: They are nearly identical for TTB$^+$ in a glassy matrix and for TTB$^+$ doped into [PPB]PF$_6$. Even the vibrational sideband energies in the luminescence spectrum of TPB$^+$ doped into [PPB]PF$_6$ do not differ much from the values of the TTB$^+$ complex. The lowest-energy excited state is obviously not strongly affected by the presence of a phpy$^-$ ligand. This is a strong indication that the luminescent state of both TTB$^+$ and TPB$^+$ is to be associated with the thpy$^-$ ligand.

In the single-crystal absorption spectra of [PPB]PF$_6$ three excited states can be identified. Their respective electronic origins are marked C, D, and N in Figure 2. On the basis of the crystal structure, it is straightforward to assign these three states to the three crystallographically nonequivalent ligands of the PPB$^+$ complex in the PF$_6^-$ salt. Since C and D have very similar energies, intensities, and vibrational sideband energies, they are assigned to the two phpy$^-$ ligands. The third excited state which corresponds to origin line N lies 967 cm^{-1} above the first excited

state C; see Table VI. It shows similar, yet significantly different, vibrational energies and is therefore assigned to the bpy ligand; see Table IV. This conclusion is further supported by the fact that a corresponding line N could also be observed for [PPB]-BPh_4 but not for $[PPE]PF_6$ and $[PPE]BPh_4$, where the bpy ligand is replaced by ethylenediamine. We conclude that in $[PPB]PF_6$ the transitions C, D, and N are essentially ligand-localized excitations. In the following we will discuss further observations which support this conclusion.

The lines C and D are observed in four salts of PPB^+ and PPE^+, as shown in Figure 3. Their energy splitting varies from 22 cm^{-1} in $[PPB]PF_6$ to 242 cm^{-1} in $[PPE]BPh_4$; see Table VI. This energy splitting reflects the influence of the slightly different environment of the two $phpy^-$ ligands in the crystal. It is thus a measure of the degree of nonequivalence of the two $phpy^-$ ligands. The orientation of the complexes with respect to the light beam is very unlikely to be the same for all the four crystal absorption spectra shown in Figure 3. But we observe that in all the spectra line C has about the same intensity as line D. There is only one reasonable explanation for this: The transition moments of C and D must be approximately parallel or antiparallel in the PPB^+ complex. In section 4.D this will be analyzed in detail.

In $[PPE]BPh_4$ we observe the largest C–D splitting of 242 cm^{-1}, implying the largest inequivalence of the two $phpy^-$ ligands imposed by the crystal environment. This is nicely confirmed by the vibrational sideband energies which are significantly different for the C and D transitions in this salt; see Table IV. In contrast, C and D were found to have the same vibrational sideband pattern in $[PPB]PF_6$, where the C–D splitting is only 22 cm^{-1}.

In Figure 3 we see that the electronic origins are accompanied by a phonon wing on their high-energy side. The relative intensity of this phonon wing, which is a measure of the electron phonon coupling strength, shows a great deal of variation. In the PPE^+ salts in particular the C and D lines carry very different phonon wings. This is yet another expression of the inequivalence of the two $phpy^-$ ligands, which couple in a slightly different manner to the lattice modes.

We also considered the possibility of excitations which are delocalized over both cyclometalating ligands. In this model the two lines C and D would be considered as a result of an electronic interaction between two local excitations. This model is not compatible with the observations discussed above.

D. Orientation of the Transition Moments for the Lowest-Energy Excitations of $[PPB]PF_6$. The integrated absorption coefficient A of a spectroscopic transition is related to the transition moment $\vec{m}$ and the electric field vector $\vec{\pi}$ of the light, according to eq 5.[36] This relation can be used to determine the molecular

$$A = \int \epsilon(\nu)\, d\nu \propto |\vec{m}\cdot\vec{\pi}|^2 \qquad (5)$$

orientation of the transition moments for the origin lines C, D, and N of $[PPB]PF_6$ from the polarized single-crystal absorption spectra. For the orthorhombic space group *Pbca* of $[PPB]PF_6$ there are eight symmetry-related complexes per unit cell and accordingly for each transition there are eight equivalent transition moments $\vec{m}_i = (\pm m_a|\pm m_b|\pm m_c)$ (i = 1–8), which differ only in the signs of their components relative to an orthonormal basis parallel to the crystal axes a, b, and c. Our experiments were performed with the electric field vector parallel to the extinction directions of the crystal, i.e. parallel to a, b, and c. The total absorption coefficient A of a given transition is obtained by adding up the contributions of the eight equivalent transition moments. For the three polarization directions the corresponding total absorption coefficients A_a, A_b, and A_c are proportional to m_a^2, m_b^2, and m_c^2, respectively. From the observed relative intensities

(36) Piepho, S. B.; Schatz, P. N. *Group Theory in Spectroscopy, With Applications to Magnetic Circular Dichroism*; Wiley-Interscience Publication, John Wiley & Sons: New York, 1983; pp 6–26.

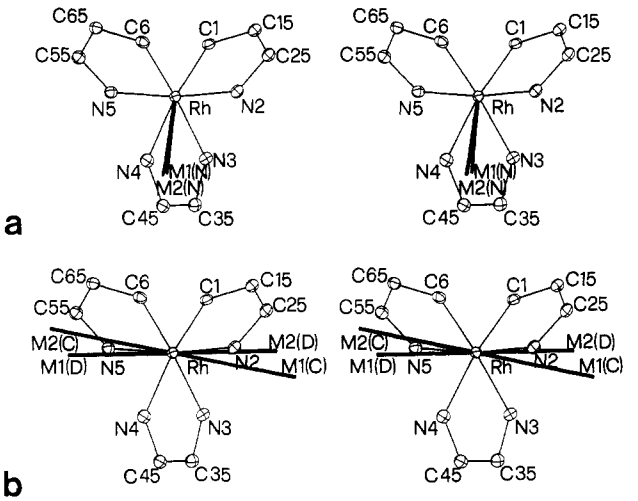

Figure 7. Molecular orientation of the observed transition moments for line N (a) and lines C and D (b) in the absorption spectra of $[PPB]PF_6$ (Figure 2). The lengths of the transition moments are proportional to the intensities of the three origin lines. Only the metal ion and the coordinating and the bridgehead atoms of the ligands are shown; see Figure 1 for the complete molecular structure of the PPB^+ complex.

of the absorption lines C, D, and N for the three polarization directions (Table V), it is therefore possible to calculate relative values for $|m_a|$, $|m_b|$, and $|m_c|$, but it is not possible to determine whether these components have a positive or a negative sign for the complex whose atomic coordinates are given in Table III. Antiparallel transition moments are physically indistinguishable. Hence, for each of the three origin lines there remain four possible orientations of the transition moments in the complex. The number of possible orientations can be further reduced by the following considerations.

(1) As the origin lines C, D, and N are ascribed to transitions which are essentially ligand-localized, we consider the symmetry properties of the ligands: (a) The bpy ligand has an approximate C_{2v} symmetry in the complex, and a transition on this ligand (corresponding to line N) is therefore either long-axis, short-axis, or out-of-plane polarized. (b) For the $phpy^-$ ligands with their approximate C_s symmetry the corresponding transition moments of the absorption lines C and D are in-plane or out-of-plane polarized.

(2) The complex still has an approximate C_2 rotation axis in the crystal lattice. The transition moments corresponding to the two origin lines C and D should therefore be approximately symmetric with respect to the pseudo-C_2 axis, because they are ascribed to equivalent localized transitions, one on the first and the other on the second of the two $phpy^-$ ligands.

(3) The transition moments corresponding to the two origin lines C and D must be nearly parallel or antiparallel to each other; see section 4.C.

Using these considerations, the structural information in Table III, and the spectroscopic data in Table V, we find for line N that it can be neither long-axis nor out-of-plane polarized. But there are two possible and very similar short-axis orientations of the transition moment for which 94% and 96%, respectively, of the total intensity of line N is ascribed to the short-axis component. These short-axis transition moments are designated $M1$(N) and $M2$(N) and are emphasized by thick lines in the stereopicture Figure 7a.

Analogous calculations for the $phpy^-$ transitions show that there are again two similar possibilities for which the conditions listed above are fullfilled. For the first of these, line C is ascribed to the $phpy^-$ ligand with atoms labeled C1–N2, and line D is ascribed to the $phpy^-$ ligand with atoms labeled N5–C6, and the corresponding transition moments are designated $M1$(C) and $M1$(D). Alternatively line C is assigned to the $phpy^-$ ligand with

atoms labeled N5–C6, and line D is ascribed to the phpy$^-$ ligand with atoms labeled C1–N2, and the corresponding transition moments are designated $M2$(C) and $M2$(D). In Figure 7b the four transition moments $M1$(C), $M1$(D), $M2$(C), and $M2$(D) are shown by the thick lines, and it can be seen that these transition moments are all in-plane polarized and oriented approximately parallel to the Rh–N bond. For both possibilities the out-of-plane contribution to the total intensity is quite small, namely 6% or 2%, respectively.

There is thus a close correspondence between the orientations of the transition moments of bpy and phpy$^-$ as far as the smallness of the out-of-plane contribution is concerned. Assuming that the general nature of the transitions localized on the phpy$^-$ ligands is similar to that localized on bpy and given the fact that the latter transition is polarized along the short axis of bpy, we expect the transitions localized on the phpy$^-$ ligands to be polarized in the respective molecular planes. This is what is observed.

This result can be understood by analyzing the intensity mechanisms of the electronic transitions. The following arguments are based on the discussion of the $^3\pi\pi^*$ state properties of [Rh(bpy)$_3$]$^{3+}$ given by Komada et al.[37] We first consider the free bpy ligand. On the basis of SCF-CI calculations, it is assumed that the orbital part of the lowest excited triplet state transforms as $B_2(\pi_{a_2}\pi^*_{b_1})$ in C_{2v}.[37,38] The spin part of the wave function transforms as B_2, B_1, and A_2 in C_{2v}. The corresponding triplet sublevels are denoted T_x, T_y and T_z, respectively, and they transform as $A_1(\pi_{a_2}\pi^*_{b_1})$, $A_2(\pi_{a_2}\pi^*_{b_1})$, and $B_1(\pi_{a_2}\pi^*_{b_1})$, respectively. For the imaginary monochelated complex [Rh(bpy)]$^{3+}$ with C_{2v} symmetry, Komada et al. have proposed the following intensity mechanisms for the three sublevels T_x, T_y, and T_z:[37] There is spin–orbit coupling to the $^1A_1(d_{b_1}\pi^*_{b_1})$ and $^1B_1(d_{a_1}\pi^*_{b_1})$ charge-transfer states for the T_x and T_z sublevels, respectively; for the T_y sublevel there is no appropriate $d\pi^*$ state for spin–orbit coupling, and the transition from this sublevel is therefore dipole-forbidden. The $d_{a_1} \rightarrow \pi^*_{b_1}$ charge-transfer intensity should be small for symmetry reasons. Hence, the T_x sublevel should dominate the $^3\pi\pi^*$ intensity. It is short-axis polarized like the $d_{b_1} \rightarrow \pi^*_{b_1}$ charge-transfer transition from which it gains its intensity. This is in gratifying agreement with the observed short-axis polarization of line N in [PPB]PF$_6$.

By completely analogous considerations we find for the phpy$^-$ ligand that the orbital part of all the $^3\pi\pi^*$ states transforms as $A'(\pi_{a''}\pi^*_{a''})$ in C_s. Intensity stealing from $d\pi^*$ states is possible for all triplet sublevels: There can be spin–orbit coupling to $^1A''(d_{a''}\pi^*_{a''})$ for T_x and T_y, which both transform as $A''(\pi_{a''}\pi^*_{a''})$, and to $^1A'(d_{a''}\pi^*_{a''})$ for T_z, which transforms as $A'(\pi_{a''}\pi^*_{a''})$. For symmetry reasons the T_z sublevel is expected to dominate the $^3\pi\pi^*$ intensity, which is in-plane polarized like the $d_{a''} \rightarrow \pi^*_{a''}$ charge-transfer transition from which it derives. Again we find agreement with the observed in-plane polarization of the origin lines C and D in [PPB]PF$_6$.

In the above model the $^3\pi\pi^*$ transitions gain their intensity through spin–orbit coupling with $^1d\pi^*$ states. The respective transition moments have the same orientations as those of the corresponding $^1d\pi^*$ transitions. As has been discussed by Day and Sanders[39] and others,[40–42] the main contribution to the transition moment of a charge-transfer transition from a donor with a d-orbital to an acceptor with a π^*-orbital of the same symmetry is ascribed to the so-called transfer term:

$$\vec{m} = \langle d|\vec{Q}|\pi^*\rangle \approx \alpha\langle\pi^*|\vec{Q}|\pi^*\rangle \qquad (6)$$

Here $\vec{Q}$ is the dipole moment operator, and α is the mixing coefficient of the d and π^* orbitals in the molecular orbital description. $\vec{m}$ is thus a vector pointing from the metal to the π^* orbital on the ligand, and for [Rh(bpy)]$^{3+}$ we immediately get the short-axis polarization. For [Rh(phpy)]$^{2+}$ we have to investigate the properties of the π^* orbital. Constable and Housecroft have performed Fenske–Hall quantum chemical calculations on phpy$^-$.[43] Their results show that the lowest unoccupied molecular orbital (LUMO) of phpy$^-$ is a π^* type orbital which is mainly localized on the pyridine ring atoms with a very small contribution from atomic orbitals of the phenyl ring atoms. The $d\pi^*$ transition moment $\vec{m}$ according to eq 6 should therefore point from the metal ion to the pyridine ring; i.e. it should be approximately parallel to the Rh–N(phpy$^-$) bond, in excellent agreement with our experimental results; see Figure 7b.

We conclude that the three absorptions C, D, and N of [PPB]PF$_6$ are essentially $^3\pi\pi^*$ transitions localized on the three ligands of the complex. They gain their intensity mainly through spin–orbit coupling with the lowest-energy $^1d\pi^*$ transitions. As was already stated in section 3.B, the polarization ratios of lines C and D of TTB$^+$ doped into [PPB]PF$_6$ are roughly the same as those of the pure host. The corresponding $^3\pi\pi^*$ transitions of the thpy$^-$ ligands are thus also polarized approximately parallel to the Rh–N(thpy$^-$) bonds, gaining their intensity through spin–orbit coupling with a $^1d\pi^*$ transition.

5. Conclusions

The combination of high-resolution single-crystal absorption, luminescence, and excitation spectroscopy provides very detailed information about the nature of the first excited states in these mixed-ligand Rh^{3+} complexes. The molecular orientation of the transition moments, derived from a combination of the polarized crystal spectra and the crystal structure, is essential for an assignment of these excitations and their intensity mechanism. The highly resolved vibrational sideband patterns are of equal importance; they are used for an unambiguous identification of the ligands involved in the transition. By the doping of a complex to be studied into a suitable host lattice, effects such as energy transfer can be suppressed[16] and its intrinsic spectroscopic properties are obtained. The spectroscopic properties of the complex TPB$^+$ can be studied by doping it into [PPB]PF$_6$ crystals without even trying to isolate it from the complex reaction mixture, which would be a formidable enterprise. By tunable laser spectroscopy the various complexes present in the mixed crystals can be selectively excited and their properties can be studied individually.

The mixed-ligand complexes of Rh^{3+} used in this study have proved to be a highly valuable source of information about the nature of photophysically and photochemically relevant first excited states. While these states can to a good approximation be considered as ligand-localized $^3\pi\pi^*$ states, in some respects the presence of Rh^{3+} nevertheless dominantes their properties. Absorption intensities to these first excited states are about 3 orders of magnitude larger than in the free ligand. Similarly their radiative luminescence decay times are shorter by about 3 orders of magnitude than in the free ligand.[5] Finally, their in-plane polarization contrasts with the out-of-plane polarization of the $^3\pi\pi^*$ transition in both the free and the protonated bpy ligand.[44,45] All these differences are due to spin–orbit coupling, which can mix a small amount of $^1d\pi^*$ character into the nominal $^3\pi\pi^*$ states and thus significantly alter their properties.

Supplementary Material Available: Text giving detailed information on the structure solution and refinement and listings of crystal measurement and refinement parameters, bond distances, bond angles, and anisotropic displacement parameters for non-hydrogen atoms (8 pages). Ordering information is given on any current masthead page.

(37) Komada, Y.; Yamauchi, S.; Hirota, N. *J. Phys. Chem.* **1986**, *90*, 6425.
(38) Hanazaki, I.; Nagakura, S. *Inorg. Chem.* **1969**, *8*, 648.
(39) Day, P.; Sanders, N. *J. Chem. Soc. A* **1967**, 1536.
(40) Ceulemans, A.; Vanquickenborne, L. G. *J. Am. Chem. Soc.* **1981**, *103*, 2238.
(41) Benedix, R.; Hennig, H. *Z. Chem.* **1988**, *28*, 367.
(42) Benedix, R.; Hennig, H. *Z. Anorg. Allg. Chem.* **1989**, *577*, 23.
(43) Constable, E. C.; Housecroft, C. E. *Polyhedron* **1990**, *9*, 1939.
(44) Okabe, N.; Ikeyama, T.; Azumi, T. *Chem. Phys. Lett.* **1990**, *165*, 24.
(45) DeArmond, M. K.; Huang, W. L.; Carlin, C. M. *Inorg. Chem.* **1979**, *18*, 3388.